Microscopic calculation of in-medium nucleon-nucleon cross sections

G. Q. Li* and R. Machleidt
Department of Physics, University of Idaho, Moscow, Idaho 83843
(Received 15 April 1993)

We derive in-medium nucleon-nucleon (NN) cross sections in a microscopic model. Our calculations are based upon the Bonn NN potential and the Dirac-Brueckner approach for nuclear matter. We consider energies up to 300 MeV (in the laboratory frame) and densities up to twice nuclear matter density. Our results deviate substantially from cross section parametrizations that are commonly used in the nuclear medium.

PACS number(s): 21.65.+f

I. INTRODUCTION

An exciting topic in contemporary nuclear physics is the study of the medium (density and/or temperature) dependence of the properties of hadrons and hadronic processes. A well-known example is the mass of the nucleon which decreases with increasing density. This is implied by relativistic (e.g., Walecka model [1,2] and Dirac-Brueckner approach [3–10]) as well as nonrelativistic (e.g., momentum dependent Skyrme forces [11,12]) models. Based on effective chiral Lagrangians, Brown, Rho, and Koch [13,14] argue that the masses of other hadrons also decrease with increasing density, at about the same rate as the mass of the nucleon. Recent finite density QCD sum rule calculations also indicate that the masses of hadrons should decrease with increasing density [15–17].

Not only the static properties of hadrons (e.g., their masses) but also the dynamical ones (e.g., two-body scattering) are modified due to the presence of the medium. In-medium nucleon-nucleon (NN) scattering differs from the corresponding one in free space, mainly due to Pauli blocking of intermediate and final states as well as the mean field. In conjunction with nucleus-nucleus collisions, Faessler and co-workers [18–20] have studied in-medium NN scattering, based on nonrelativistic Brueckner calculations and the Reid soft-core potential. This approach has been applied in calculations of the nucleus-nucleus optical potential at low energies [18–21] and in the transport model description of nucleus-nucleus collisions at intermediate energies [22–24]. It should, however, be emphasized that nonrelativistic many-body theory, e.g., the Brueckner approach [25–27] and the variational method [28–30], is not able to reproduce correctly the saturation properties (saturation density and energy) of nuclear matter, when two-body forces are applied [5].

The investigation of in-medium NN scattering is of interest for intermediate-energy heavy-ion reactions. Experimentally, nucleus-nucleus collisions at intermediate energies provide a unique opportunity to form a piece of nuclear matter in the laboratory with a density up to $(2\text{–}3)\rho_0$ (with ρ_0, in the range of 0.15–0.19 fm^{-3}, the saturation density of normal nuclear matter; in this paper we use ρ_0=0.18 fm^{-3}) [31,32]. Thus it is possible to study the properties of hadrons in a dense medium. Since this piece of dense nuclear matter exists only for a very short time (typically 10^{-23}–10^{-22} s), it is necessary to use transport models to simulate the entire collision process and to deduce the properties of the intermediate stage from the known initial conditions and the final-state observables. At intermediate energies, both the mean field and the two-body collisions play an equally important role in the dynamical evolution of the colliding system; they have to be taken into account in the transport models on an equal footing, together with a proper treatment of the Pauli blocking for the in-medium two-body collisions. The Boltzmann-Uehling-Uhlenbeck (BUU) equation [33,34] and quantum molecular dynamics (QMD) [35,36], as well as their relativistic extensions (RBUU and RQMD) [17,37–40], are promising transport models for the description of intermediate-energy heavy-ion reactions. In addition to the mean field, the in-medium NN cross section is also an important ingredient of these transport models. Specifically, the in-medium total as well as differential NN cross sections are needed by these models in dealing with the in-medium NN scattering using a Monte Carlo method. Moreover, if these models are used to calculate the spectrum of particles produced in heavy-ion collisions, such as photons, pions, and kaons, one also needs to know the in-medium elementary particle production cross section [34,38,41–44]; e.g., the in-medium cross section of neutron-proton (np) bremsstrahlung ($np \to np\gamma$) is needed in the calculation of the photon production cross section in nucleus-nucleus collisions. Up until now, most calculations of particle production in nucleus-nucleus collisions are based on the free production cross sections.

It is the purpose of this paper to calculate the elastic in-medium NN cross sections in a microscopic way. We base our investigation on the Bonn meson-exchange model for the NN interaction [5,45] and the Dirac-Brueckner approach [5–7] for nuclear matter.

Speaking in more general terms, it is the fundamental goal of traditional nuclear physics to describe nuclear structure and nuclear reactions in terms of the same realistic NN interaction. This bare interaction should be based as much as possible on theory and describe the two-nucleon system (NN scattering as well as the deuteron)

*Present address: Cyclotron Institute, Texas A&M University, College Station, TX 77843.

accurately.

There are two aspects to the problem. First, one needs a realistic NN interaction which is ultimately determined by the underlying dynamics of quarks and gluons and should in principle be derived from quantum chromodynamics (QCD). However, due to the nonperturbative character of QCD in the low-energy regime relevant for nuclear physics, we are far away from a quantitative understanding of the NN interaction in this way. On the other hand, there is a good chance that conventional hadrons, such as nucleons and mesons, remain the relevant degrees of freedom for a wide range of low-energy nuclear physics phenomena. In that case, the overwhelming part of the NN potential can be constructed in terms of meson-baryon interactions. In fact, the only quantitative NN interactions available up until now are based upon the idea of meson exchange; two well-known examples are the Paris potential [46,47] and the Bonn potential [5,45] (see Ref. [5] for a comprehensive overview of the history of meson-exchange models).

The second aspect of the problem concerns a suitable many-body theory that is able to deal with the bare NN interaction which has a strong repulsive core. The Brueckner approach [25–27] and variational method [28–30] have been developed for this purpose. However, when using two-body forces, the Brueckner approach and the variational method are not able to reproduce correctly the saturation properties of nuclear matter. Inspired by the success of the Dirac phenomenology in intermediate-energy proton-nucleus scattering [48–50] and the Walecka model [quantum hydrodynamics (QHD)] for dense nuclear matter [1,2], a relativistic extension of the Brueckner approach has been initiated by Shakin and co-workers [3,4], frequently called the Dirac-Brueckner approach. This approach has been further developed by Brockmann and Machleidt [5,6,51] and by ter Haar and Malfliet [8–10]. Formal aspects involved in the derivation of the relativistic G matrix have been discussed in detail by Horowitz and Serot [52,53]. The common feature of all Dirac-Brueckner results is that a repulsive relativistic many-body effect is obtained which is strongly density dependent such that the empirical nuclear matter saturation can be explained. The Dirac-Brueckner approach thus provides a reasonable starting point for pursuing the longstanding goal of self-consistently describing nuclear matter, finite nuclei, and nuclear reactions based on the same realistic NN interaction. The extension of this relativistic approach to the domain of finite nuclei has been discussed by Müther *et al.* [54] and recently by Brockmann and Toki [55], while the investigation of nucleon-nucleus scattering has been initiated by Nuppenau *et al.* [56].

This paper is the first in a series in which we investigate systematically in-medium NN scattering based on the Bonn potential and the Dirac-Brueckner approach. In this paper, we are concerned with elastic in-medium NN scattering which is the most important two-body process in nucleus-nucleus collisions at incident energy below 300 MeV per nucleon. In Sec. II we give a brief description of the Bonn potential and compare theoretical predictions with experimental data for free-space NN scattering. The Dirac-Brueckner approach and the predictions for nuclear matter are discussed in Sec. III. The results for the in-medium NN cross sections are presented and discussed in Sec. IV. Finally we give a brief summary and outlook in Sec. V.

II. BONN MODEL AND NN OBSERVABLES

Two-nucleon scattering is described covariantly by the Bethe-Salpeter equation [57]. As this four-dimensional integral equation is very difficult to solve, so-called three-dimensional reductions have been proposed, which are more amenable to numerical solution [58,59]. Among the different forms of three-dimensional reductions, the one suggested by Thompson [59] is particularly suitable for the relativistic many-body problem [5,6]. In terms of the R matrix (or K matrix) the Thompson equation reads, in the center-of-mass system [60],

$$R(\mathbf{q}',\mathbf{q}) = V(\mathbf{q}',\mathbf{q}) + \mathcal{P}\int \frac{d^3k}{(2\pi)^3} V(\mathbf{q}',\mathbf{k}) \frac{m^2}{E_k^2} \frac{1}{2E_q - 2E_k} R(\mathbf{k},\mathbf{q}), \tag{1}$$

where $\mathbf{q}$, $\mathbf{k}$, and $\mathbf{q}'$ are initial, intermediate, and final relative momenta, respectively, of the two scattering nucleons. $E_q = (m^2 + \mathbf{q}^2)^{1/2}$ with m the mass of the free nucleon. $\mathcal{P}$ denotes the principal value.

In the one-boson-exchange (OBE) model, the kernel of this integral equation, $V(\mathbf{q}',\mathbf{q})$, is the sum of one-particle-exchange amplitudes of certain bosons with given mass and coupling. In the OBE Bonn model [5], six nonstrange bosons with mass below 1 GeV are used; they are pseudoscalar mesons (π and η), scalar mesons (δ and σ), and vector mesons (ρ and ω). The meson-nucleon interactions are described by the Lagrangians

$$\mathcal{L}_{pv} = -\frac{f_{ps}}{m_{ps}} \overline{\psi}\gamma^5\gamma^\mu\psi\partial_\mu\phi^{(ps)}, \tag{2}$$

$$\mathcal{L}_s = g_s \overline{\psi}\psi\phi^{(s)}, \tag{3}$$

$$\mathcal{L}_v = -g_v \overline{\psi}\gamma^\mu\psi\phi_\mu^{(v)} - \frac{f_v}{4m}\overline{\psi}\sigma^{\mu\nu}\psi(\partial_\mu\phi_\nu^{(v)} - \partial_\nu\phi_\mu^{(v)}), \tag{4}$$

with ψ the nucleon and $\phi_{(\mu)}^{(\alpha)}$ the meson fields (notation and convention as in Ref. [61]). For isospin-1 mesons (π, δ, and ρ), $\phi^{(\alpha)}$ is to be replaced by $\tau\cdot\phi^{(\alpha)}$, with τ the usual Pauli matrices. Note that the pseudovector coupling is used for pseudoscalar mesons in order to avoid unrealistically large antiparticle contributions.

From the above Lagrangians, we can derive the OBE amplitudes; e.g., the contribution from the isoscalar-scalar meson is given by

$$\langle \mathbf{q}'\lambda_1'\lambda_2'|V_s^{\rm OBE}|\mathbf{q}\lambda_1\lambda_2\rangle = -g_s^2 \overline{u}(\mathbf{q}',\lambda_1')u(\mathbf{q},\lambda_1)\overline{u}(-\mathbf{q}',\lambda_2')u(-\mathbf{q},\lambda_2)\frac{\{\mathcal{F}_s[(\mathbf{q}'-\mathbf{q})^2]\}^2}{(\mathbf{q}'-\mathbf{q})^2 + m_s^2}, \tag{5}$$

TABLE I. Parameters of the OBE Bonn potentials used in this work (reprinted from Ref. [5], Appendix A, Table A.2, therein).

		Bonn A		Bonn B		Bonn C	
Mesons	m_α (MeV)	$g_\alpha^2/4\pi$	Λ_α (GeV)	$g_\alpha^2/4\pi$	Λ_α (GeV)	$g_\alpha^2/4\pi$	Λ_α (GeV)
π^a	138.03	14.9	1.05	14.6	1.2	14.6	1.3
η^a	548.8	7	1.5	5	1.5	3	1.5
ρ^b	769	0.99	1.3	0.95	1.3	0.95	1.3
ω^b	782.6	20	1.5	20	1.5	20	1.5
δ	983	0.7709	2.0	3.1155	1.5	5.0742	1.5
σ	550	8.3141	2.0	8.0769	2.0	8.0279	1.8

[a] $g_\alpha = \frac{2m}{m_\alpha} f_\alpha$ for π and η.

[b] We use $\frac{f_\rho}{g_\rho}$=6.1 and $\frac{f_\omega}{g_\omega}$=0.

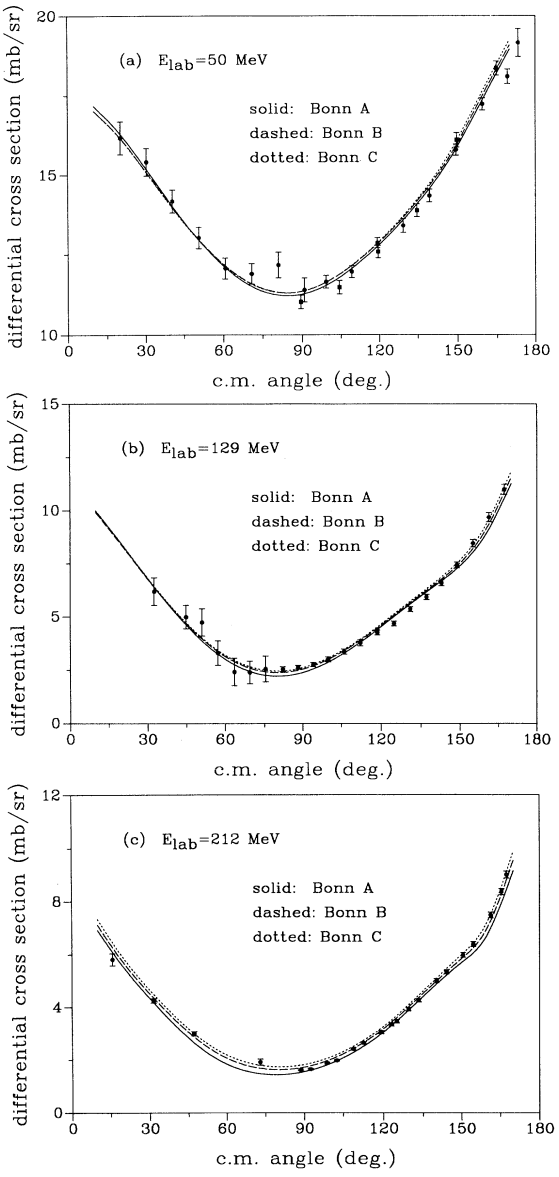

FIG. 1. Neutron-proton differential cross sections at (a) 50 MeV, (b) 129 MeV, and (c) 212 MeV. The curves are predictions by the Bonn potentials. The data at 50 MeV are from Ref. [62] (solid circles) and Ref. [63] (solid squares), while the data at 129 MeV and 212 MeV are from Ref. [64] and Ref. [65], respectively.

where λ_i (λ_i'), with $i = 1, 2$, denotes the helicity of the incoming (outgoing) nucleons. $\mathcal{F}_s[(\mathbf{q}' - \mathbf{q})^2]$ is a form factor of monopole type which simulates the short-range physics governed by quark-gluon dynamics:

$$\mathcal{F}_s[(\mathbf{q}' - \mathbf{q})^2] = \frac{\Lambda_s^2 - m_s^2}{\Lambda_s^2 + (\mathbf{q}' - \mathbf{q})^2}, \tag{6}$$

with Λ_s the cutoff mass of the isoscalar-scalar meson. The Dirac spinors are normalized covariantly:

$$\overline{u}(\mathbf{q}, \lambda) u(\mathbf{q}, \lambda) = 1. \tag{7}$$

The OBE amplitudes for other mesons are given in Refs. [5,45,60].

Three sets of OBE potential parameters, denoted by Bonn A, B, and C, have been proposed [5]. We reprint them in Table I. The main difference between the three parameter sets is the cutoff parameter for the πNN vertex, which is 1.05, 1.2, and 1.3 GeV for Bonn A, B, and C, respectively. Consequently, the three potentials differ in their strength of the tensor force component which is not well constrained by present NN data. Bonn A has the weakest tensor force and Bonn C the strongest. All

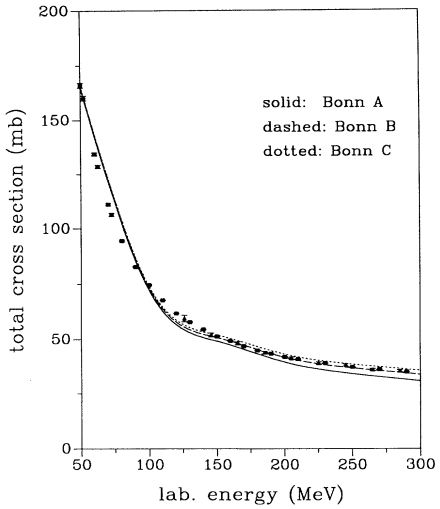

FIG. 2. Neutron-proton total cross sections in the energy range 50–300 MeV. The curves are the predictions by the Bonn potentials. The data are from Ref. [66] (solid circles), Ref. [67] (solid triangles), and Ref. [68] (solid squares).

three potentials reproduce the deuteron properties and the phase shifts of NN scattering up to about 300 MeV accurately (cf. Refs. [5,6]).

Our goal is to calculate the in-medium NN cross sections microscopically. For this purpose it is important that the bare NN interaction describe the free NN scattering cross sections correctly. In Fig. 1, we compare the predictions by the Bonn potentials with the neutron-proton (np) differential cross section data at 50, 129, and 212 MeV. It is seen that all three potentials reproduce the data very well. In Fig. 2 we show the np total cross sections in the energy range 50–300 MeV. There is good agreement between theory and experiment.

III. DIRAC-BRUECKNER APPROACH AND NUCLEAR MATTER PROPERTIES

As mentioned in the Introduction, the essential point of the Dirac-Brueckner approach is the use of the Dirac equation for the description of the single-particle motion in the nuclear medium,

$$[\boldsymbol{\alpha}\cdot\mathbf{k}+\beta(m+U_S)+U_V]\tilde{u}(\mathbf{k},s)=\epsilon_k\tilde{u}(\mathbf{k},s), \tag{8}$$

where U_S is an attractive scalar field and U_V the timelike component of a repulsive vector field. m is the experimental mass of the free nucleon. The solution of this equation is

$$\tilde{u}(\mathbf{k},s)=\left(\frac{\tilde{E}_k+\tilde{m}}{2\tilde{m}}\right)^{1/2}\begin{pmatrix}1\\ \frac{\boldsymbol{\sigma}\cdot\mathbf{k}}{\tilde{E}_k+\tilde{m}}\end{pmatrix}\chi_s, \tag{9}$$

with

$$\tilde{m}=m+U_S,$$

$$\tilde{E}_k=(\tilde{m}^2+\mathbf{k}^2)^{1/2},$$

and χ_s is a Pauli spinor. Note that the in-medium Dirac spinor is obtained from the free Dirac spinor by replacing m by $\tilde{m}$.

The single-particle energy resulting from Eq. (8) is

$$\epsilon_k=\tilde{E}_k+U_V\ . \tag{10}$$

Similar to conventional Brueckner theory, the basic quantity in the Dirac-Brueckner approach is a $\tilde{G}$ matrix which satisfies the in-medium Thompson equation (also known as relativistic Bethe-Goldstone equation) [5–7], which reads, in the nuclear matter rest frame,

$$\tilde{G}(\mathbf{q}',\mathbf{q}|\mathbf{P},\tilde{z})=\tilde{V}(\mathbf{q}',\mathbf{q})+\mathcal{P}\int\frac{d^3k}{(2\pi)^3}\tilde{V}(\mathbf{q}',\mathbf{k})\frac{\tilde{m}^2}{\tilde{E}^2_{(1/2)\mathbf{P}+\mathbf{k}}}\frac{Q(\mathbf{k},\mathbf{P})}{\tilde{z}-2\tilde{E}_{(1/2)\mathbf{P}+\mathbf{k}}}\tilde{G}(\mathbf{k},\mathbf{q}|\mathbf{P},\tilde{z}), \tag{11}$$

with

$$\tilde{z}=2\tilde{E}_{(1/2)\mathbf{P}+\mathbf{q}}$$

and $\mathbf{P}$ is the c.m. momentum of the two colliding nucleons in the nuclear medium. Equation (11) is density dependent which is suppressed in our notation. Notice that in the energy denominator of Eq. (11) [which is the difference of single-particle energies of the kind Eq. (10)], U_V drops out since it is constant.

The in-medium Thompson equation differs from the free one mainly in three points [comparing Eq. (11) with Eq. (1)]. First, the Pauli operator Q prevents scattering into occupied intermediate states ("Pauli effect"). Note that this is different from the Pauli blocking factor for the final states which is always included in the transport models describing nucleus-nucleus collisions. Second, the nucleon mean field due to the medium reduces the mass of the nucleon and affects the energy denominator in Eq. (11) which is now density dependent, while in Eq. (1) the energy denominator uses free relativistic energies ("dispersion effect"). Finally and most importantly, the potential used in the in-medium Thompson equation, as indicated by the tilde, is evaluated by using the in-medium Dirac spinors of Eq. (9) instead of the free ones that are used for the V in Eq. (1). This leads to the suppression of the attractive σ exchange which increases with density. The fact that the Dirac-Brueckner approach is able to reproduce quantitatively the saturation properties of nuclear matter is mainly due to this relativistic effect. This observation also implies that the in-medium NN cross sections based on the nonrelativistic Brueckner approach lack one important aspect [20,22,23], namely, the effect which is due to the medium modification of the potential.

The scalar and vector fields of the Dirac equation (8) are determined from

$$\frac{\tilde{m}}{\tilde{E}_i}U_S+U_V=\sum_{j\le k_F}\frac{\tilde{m}^2}{\tilde{E}_i\tilde{E}_j}\langle ij|\tilde{G}(\tilde{z})|ij-ji\rangle, \tag{12}$$

which is the relativistic analog to the nonrelativistic Brueckner-Hartree-Fock definition of a single-particle potential.

Since the kernel of the in-medium Thompson equation [Eq. (11)] depends on the solution of the Dirac equation [Eq. (8)], while for the Dirac equation one needs the scalar and vector potentials which are related to the $\tilde{G}$ matrix via Eq. (12), one has to carry out an iterative procedure with the goal to achieve self-consistency of the two equations [5–7]: Starting from reasonable initial values for $U_S^{(0)}$ and $U_V^{(0)}$, one solves the in-medium Thompson equation in momentum space by means of the matrix inversion method [71] to get the $\tilde{G}$ matrix which

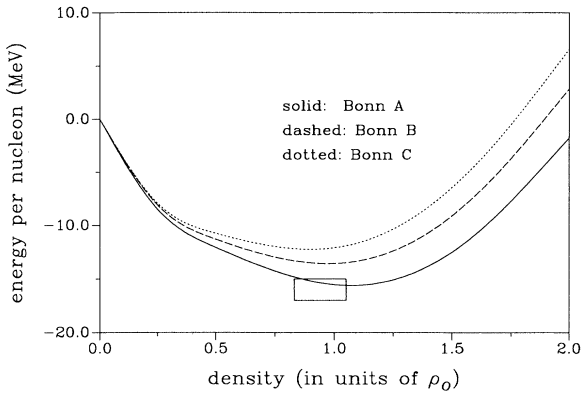

FIG. 3. Energy per nucleon in nuclear matter as obtained in the Dirac-Brueckner approach using the Bonn potentials. The box denotes the empirical region of nuclear matter saturation.

leads by means of Eq. (12) to a new set of values for $U_S^{(1)}$ and $U_V^{(1)}$ to be used in the next iteration; this procedure is continued until convergence is achieved.

The nuclear equation of state, that is, the energy per nucleon, $\mathcal{E}/\mathrm{A}$, as a function of density, ρ, is obtained from the $\tilde{G}$ matrix [5,6]:

$$\frac{\mathcal{E}}{A} = \frac{1}{A}\sum_{i\le k_F} \frac{m\tilde{m}+\mathbf{p}_i^2}{\tilde{E}_i} + \frac{1}{2A}\sum_{i,j\le k_F} \frac{\tilde{m}^2}{\tilde{E}_i\tilde{E}_j}\langle ij|\tilde{G}(\tilde{z})|ij-ji\rangle - m. \quad (13)$$

We show in Fig. 3 the energy per nucleon $\mathcal{E}/A$ as function of nuclear matter density, ρ/ρ_0 (ρ_0=0.18 fm^{-3}). The solid, dashed, and dotted lines are the results corresponding to the Bonn A, B, and C potentials, respectively. The open rectangle indicates the empirical region for nuclear matter saturation. There is some difference between the results obtained with the different potentials, especially for the nuclear equation of state at higher densities, although these potentials predict the same in free-space NN scattering. This difference can be traced back to differences in the strength of the tensor force, as reflected in the predictions for the D-state probability, P_D, of the deuteron [5,45,70]. The Bonn A potential, with the lowest D-state probability (P_D=4.47%), indicating a weak tensor force, yields the best prediction for the empirical values of nuclear matter saturation. More results and discussion of the properties of (dense) nuclear matter and neutron matter can be found in Refs. [5–7].

IV. IN-MEDIUM NN CROSS SECTIONS

In the previous sections, we discussed briefly the Bonn potentials, their predictions for free-space NN scattering, and the Dirac-Brueckner approach for nuclear matter. The potentials describe free-space NN scattering accurately and nuclear matter saturation is reproduced well in the Dirac-Brueckner approach (especially with the Bonn A potential).

In-medium NN cross sections can be calculated directly from the $\tilde{G}$ matrix [22,9,69]. Alternatively, one can also calculate first the in-medium phase shifts, which are defined in terms of the partial-wave $\tilde{G}$-matrix elements like the free-space NN phase shifts are defined in terms of the R-matrix [60] elements. From the in-medium phase shifts, the in-medium NN cross sections are obtained in the usual way.

We calculate the $\tilde{G}$ matrix, from which we obtain the in-medium cross sections, in the center-of-mass (c.m.) frame of the two interacting nucleons; i.e., we use Eq. (11) with $\mathbf{P}=0$. For the starting energy in Eq. (11), we have now $\tilde{z} = 2\tilde{E}_q = 2\sqrt{\tilde{m}^2+q^2}$, where q is related to the kinetic energy of the incident nucleon in the "laboratory system" ($E_{\rm lab}$), in which the other nucleon is at rest, by $E_{\rm lab} = 2q^2/m$. Thus, we consider two colliding nucleons in nuclear matter. The Pauli projector is represented by one Fermi sphere as in conventional nuclear matter calculations. This Pauli projector, which is originally defined in the nuclear matter rest frame, must be boosted to the c.m. frame of the two interacting nucleons. For a detailed discussion of this and the explicit formulae, see Refs. [8,53]. In summary, for in-medium NN scattering K matrix, we use the $\tilde{G}$ matrix of Eq. (11) with $\mathbf{P}=0$, $\tilde{z}=2\tilde{E}_q$, and the Pauli projector Q replaced by the ellipsoidal one due to Lorentz boosting.

In Fig. 4 we show the in-medium np phase shifts for the $^1S_0$, $^3P_0$, and $^3S_1$ partial-wave states as a function of the laboratory energy. For each partial wave, we present three different results corresponding to density ρ=0 (free-space scattering, solid lines), ρ_0 (dashed lines), and $2\rho_0$ (dotted lines). The results presented in this figure are obtained with the Bonn A potential. A clear decrease of the NN phase shifts with increasing density is observed. This is due to the Pauli and dispersion effect as well as the relativistic medium effects.

In Fig. 5 we show the results for the in-medium np differential cross sections as a function of the c.m. angle for $E_{\rm lab}$=50, 100, 250, and 300 MeV. For each incident energy, we present four different results corresponding to the medium density ρ=0 (free-space scattering, solid lines), $(1/2)\rho_0$ (long-dashed lines), ρ_0 (short-dashed lines), and $2\rho_0$ (dotted lines). The results are obtained by using the Bonn A potential. At low incident energies [Figs. 5(a) and 5(b)], the np differential cross section always decreases with increasing density, at both forward and backward angles. At high incident energies [Figs. 5(c) and 5(d)], the np differential cross section for forward angles decreases when going from ρ=0 to $(1/2)\rho_0$ and then increases for higher densities. The differential cross section at backward angles always decreases with density. While the free np differential cross sections are highly anisotropic, the in-medium cross sections become more isotropic with increasing density.

In Fig. 6, we compare the in-medium np differential cross sections as predicted by different potentials. The cross sections in free space are shown in Fig. 6(a), while Figs. 6(b) and 6(c) display them for $\rho=\rho_0$ and $\rho=2\rho_0$, respectively. The incident energy is fixed at 100 MeV. While the predictions for the np differential cross section

in free space are essentially the same, these potentials lead to slightly different in-medium np differential cross sections at higher densities [see Figs. 6(b) and 6(c)]: At $\rho = \rho_0$, the prediction by the Bonn A potential is larger than those by Bonn B and C in all directions, while at $\rho = 2\rho_0$, the prediction by the Bonn A potential is smallest in the forward direction and largest in the backward direction. This difference is mainly due to differences in the strength of the tensor potential. The purpose of Fig. 6 is to give some idea of the model dependence in our approach, due to our incomplete knowledge of the nuclear force. Fortunately, this model dependence turns out to be quite moderate.

It is also interesting to compare the results obtained in

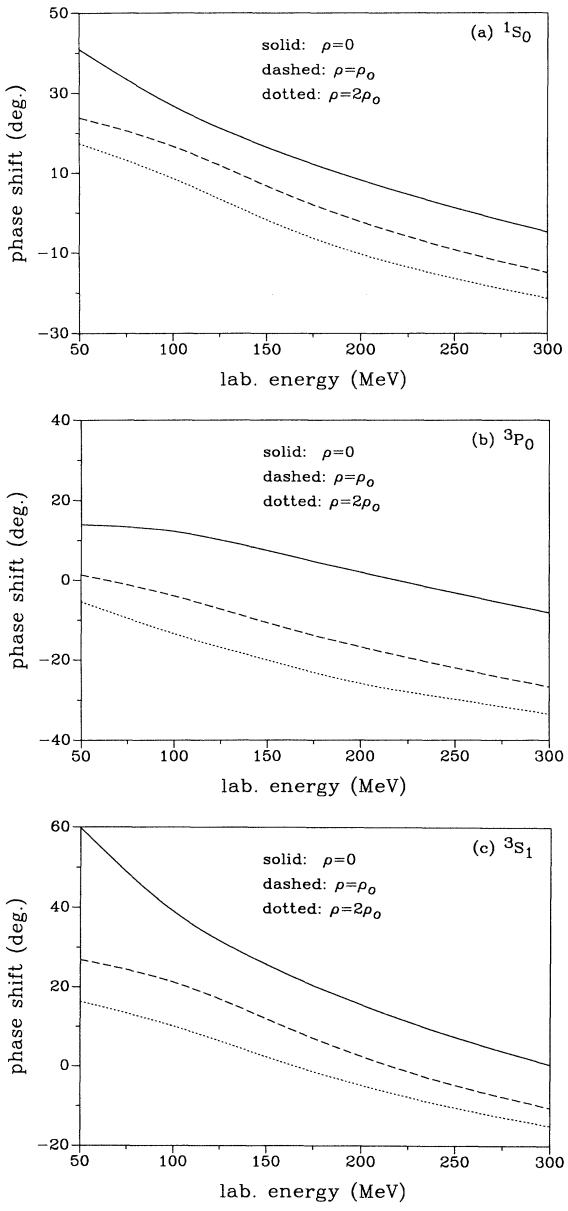

FIG. 4. In-medium np phase shifts for (a) $^1S_0$, (b) $^3P_0$, and (c) $^3S_1$. The results are obtained with the Bonn A potential.

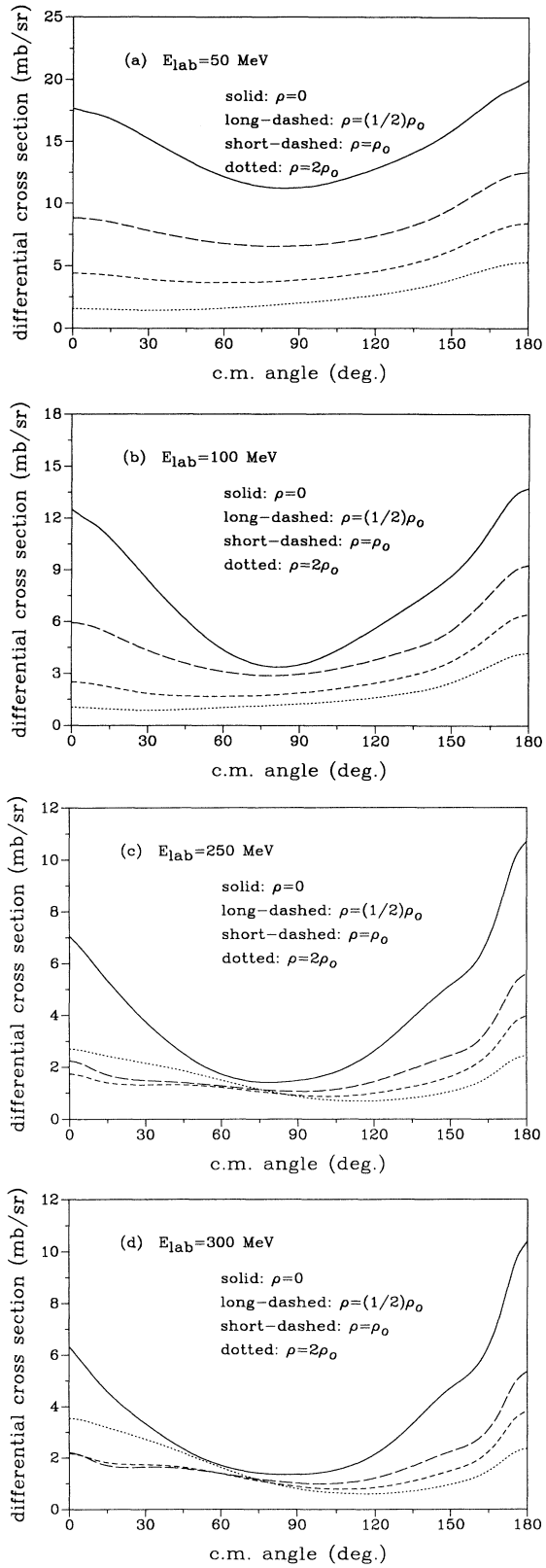

FIG. 5. In-medium np differential cross sections at (a) 50 MeV, (b) 100 MeV, (c) 250 MeV, and (d) 300 MeV laboratory energy, as obtained for various densities. The Bonn A potential is used.

this work with the parametrized NN cross sections proposed by Cugnon *et al.* [72] which are often used in transport models such as BUU [33] and QMD. This is done in Fig. 7 for a laboratory energy of 300 MeV. We compare our predictions for three different densities (using the Bonn A potential) with the parametrization of Cugnon *et al.* It is clearly seen that, while the parametrization of Cugnon *et al.* is almost isotropic, the microscopic results still have some anisotropy at all densities considered. The anisotropy in the present results decreases with increasing density (mainly due to the decrease of the magnitude

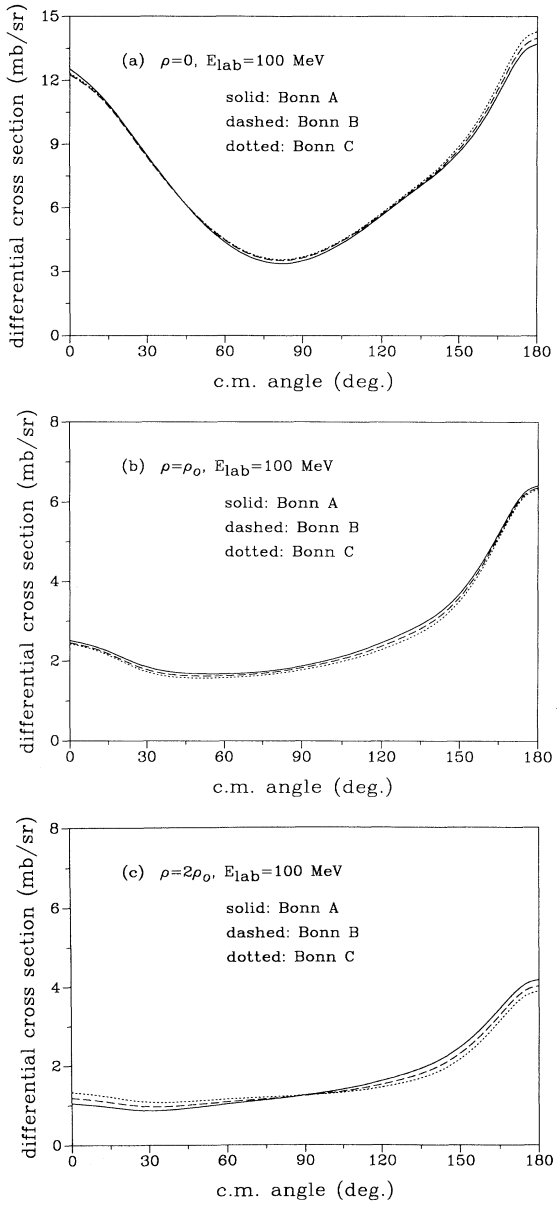

FIG. 6. In-medium np differential cross sections at 100 MeV laboratory energy for the densities (a) ρ=0, (b) $\rho = \rho_0$, and (c) $\rho = 2\rho_0$. Predictions by three differential potentials are shown.

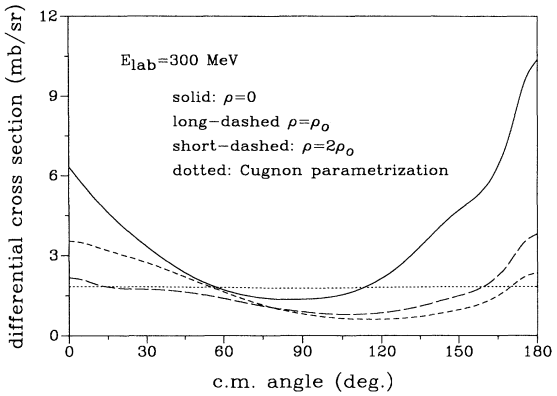

FIG. 7. In-medium np differential cross section at 300 MeV laboratory energy for the densities $\rho = 0$, $\rho = \rho_0$, and $\rho = 2\rho_0$, using the Bonn A potential. The dotted curve is the parametrization of Cugnon *et al.* [72].

of the $^1P_1$ phase shift). There is also density dependence in the microscopic differential cross section, while the parametrization of Cugnon *et al.* is density independent.

We mention that Cugnon *et al.* [72] have parametrized the free pp cross sections. This explains the almost isotropy in their differential cross sections as well as the lack of the density dependence. Note that in the work of Cugnon *et al.* [72] no difference is made between proton and neutron; thus, the pp cross sections are also used for np scattering. There are, however, well-known differences between pp and np cross sections which in the more accurate microscopic calculations of the near future may be relevant. The difference between the (in-medium) np and pp cross sections will be discussed in detail in a forthcoming paper [73]. In this paper, all "NN cross sections" are np cross sections.

The np differential cross section in free space can be well parametrized by the following simple expression:

$$\frac{d\sigma}{d\Omega}(E_{\rm lab},\theta) = \frac{17.42}{1.0 + 0.05(E_{\rm lab}^{0.7} - 15.5)} \times \exp\left[b\left(\cos^2\theta + \sin^2\frac{\theta}{7} - 1.0\right)\right], \quad (14)$$

with

$$b = 0.0008(E_{\rm lab}^{0.54} - 4.625) \quad \text{for} \quad E_{\rm lab} \leq 100 \text{ MeV}$$

and

$$b = 0.0006(36.65 - E_{\rm lab}^{0.58}) \quad \text{for} \quad E_{\rm lab} > 100 \text{ MeV},$$

with $E_{\rm lab}$ in the units of MeV.

The quality of this parametrization is demonstrated in Fig. 8, where it is compared with the microscopic results (points) based on Bonn A at three energies. It would be useful to parametrize the in-medium np differential cross section as well. However, the complicated dependence of the in-medium differential cross sections on angles, energy, and especially density makes this very

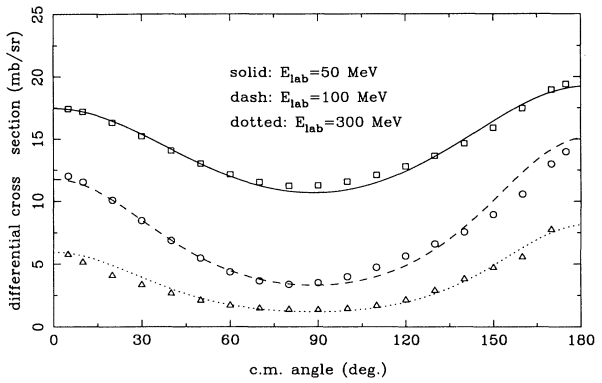

FIG. 8. Free-space np differential cross sections at three energies. The lines are the predictions by the parametrization, Eq. (14); the squares, circles, and triangles are the microscopic results at $E_{\rm lab}$=50, 100, and 300 MeV, respectively, as predicted by the Bonn A potential.

difficult. Instead, we have prepared a data file, containing in-medium differential cross sections as a function of angle for a number of densities and energies, from which the differential cross sections for all densities in the range $(0–3)\rho_0$ and all energies in the range 0–300 MeV can be interpolated. This data file is available from the authors upon request.

In addition to the in-medium NN differential cross sections which enter the transport models to determine the direction of the outgoing nucleons, the in-medium total NN cross sections, σ_{NN}, are also of interest. They provide a criterion for whether a pair of nucleons will collide or not by comparing their closest distance to $\sqrt{\sigma_{NN}/\pi}$. We show in Fig. 9(a) the in-medium total cross sections as function of the incident energy $E_{\rm lab}$ and in Fig. 9(b) as function of density. For completeness, we also list in Table II the microscopic in-medium np total cross sections as function of density and energy. All results are obtained by using the Bonn A potential.

It is seen that the in-medium total cross sections decrease substantially with increasing density, particularly for low incident energies. This agrees well with the findings of Ref. [9], but disagrees with Ref. [22]. In Ref. [22], an enhancement of the cross section was found below 150 MeV and little change (as compared to the free cross section) above 150 MeV. The major difference between our (and Ref. [9]) calculations and the ones of Ref. [22] is that we include relativistic many-body effects, which are ignored in Ref. [22]. Besides this, we as well as Ref. [22] include the Pauli and dispersion effects (which are larger than the relativistic effects). The latter two effects reduce considerably the magnitude of, in particular, the $^1S_0$ and $^3S_1$ G-matrix elements. This fact is well known since the work of Bethe and his group on Brueckner theory in the 1960s [74]. This leads to a substantial reduction of the binding energy in nuclear matter as well as the in-medium NN cross sections, since both are based upon the G matrix. On the background of these well-established facts, it is hard to understand the results of Ref. [22], while our results and the ones of Ref. [9] are physically quite meaningful.

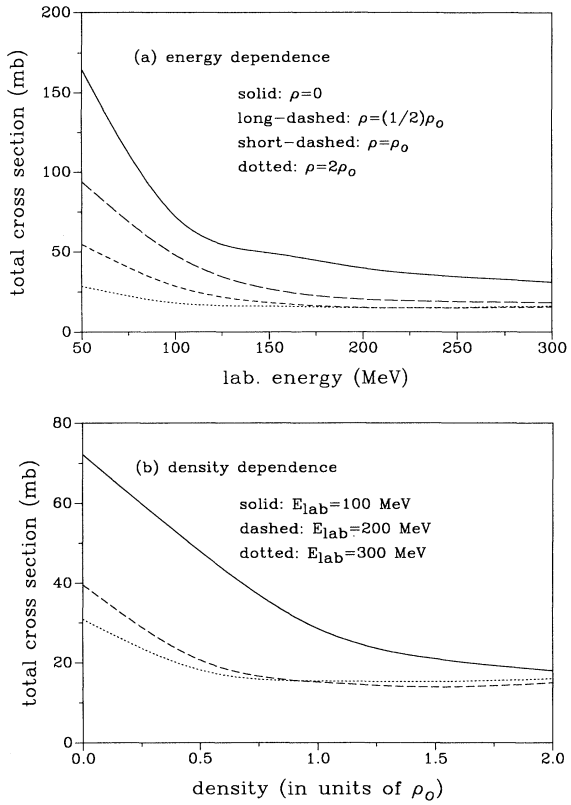

FIG. 9. In-medium np total cross sections (a) as function of the incident energy and (b) as function of density. The results are obtained with the Bonn A potential.

At higher energies ($\approx$ 300 MeV), the medium effect becomes smaller as compared to lower energies [cf. Fig. 9(a)], but it does not vanish. We use the continuous choice for the single-particle potential, and so there is a dispersive effect also for higher momenta; in addition, there are the relativistic effects. This explains the non-negligible medium effects at intermediate energies. Again, in this we agree with Ref. [9], and disagree with Ref. [22] where above 150 MeV the free cross sections were obtained. The use of the "gap choice" for the single-particle spectrum (i.e., free energies above the Fermi surface) and the omission of relativistic effects in Ref. [22] may be the explanation here.

In Fig. 10 we compare the total in-medium cross sections obtained with different potentials. Figures 10(a) and 10(b) correspond to the density $\rho = \rho_0$ and $2\rho_0$, re-

TABLE II. Microscopic in-medium np cross section $\sigma_{\rm tot}$ (mb) obtained in this work with Bonn A. ρ_0=0.18 fm^{-3}.

	$E_{\rm lab}$ (MeV)					
ρ	50	100	150	200	250	300
0	164.8	72.18	49.17	39.57	34.27	30.85
$(1/2)\rho_0$	93.92	47.96	26.71	20.62	18.76	18.14
ρ_0	54.67	28.50	18.17	15.14	14.93	15.40
$(3/2)\rho_0$	37.76	20.93	15.53	13.91	14.41	15.26
$2\rho_0$	28.48	17.96	15.96	14.94	15.14	15.97

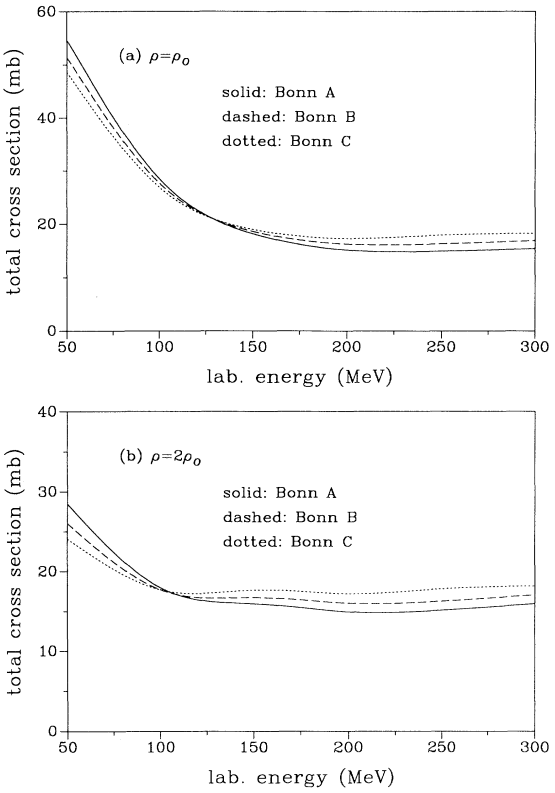

FIG. 10. In-medium np total cross sections as predicted by different potentials at densities (a) $\rho = \rho_0$ and (b) $\rho = 2\rho_0$.

spectively. The solid, dashed, and dotted lines refer to Bonn A, B, and C, respectively. By comparing Fig. 10 with Fig. 2 we see that, although the potentials lead to essentially the same predictions in free space, there is some difference in the medium, and this difference increases with density. The prediction by the Bonn A potential is the largest at low energies and the smallest at high energies. Again, fortunately, the model dependence is moderate.

We compare in Fig. 11 the total in-medium cross sec-

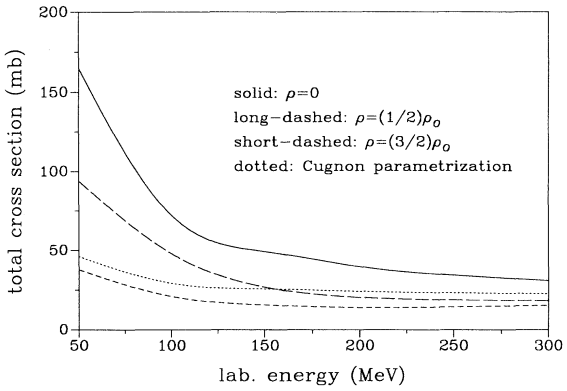

FIG. 11. In-medium np total cross sections as described by the parametrization of Cugnon *et al.* [72] (dotted line) are compared with the predictions by our microscopic calculation using the Bonn A potential.

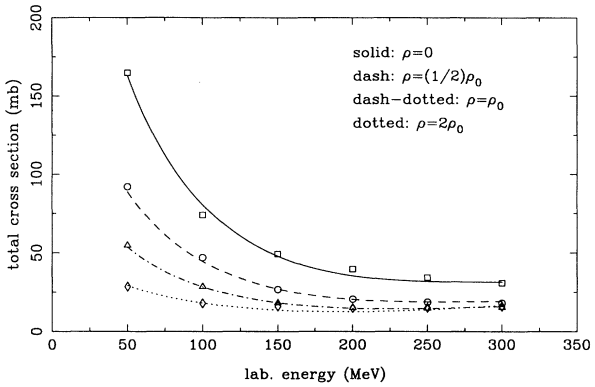

FIG. 12. In-medium np total cross section as function of incident energy at four densities. The curves are the description by the parametrization, Eq. (15); the squares, circles, triangles, and diamonds are the microscopic results at $\rho = 0$, $(1/2)\rho_0$, ρ_0, and $2\rho_0$, respectively, using the Bonn A potential.

tion obtained in the present work using the Bonn A potential with the one used by Bertsch and Das Gupta [33] and Cugnon *et al.* [72]. The solid, long-dashed, and short-dashed lines are the present results corresponding to the medium densities $\rho = 0$, $1/2\rho_0$, and $3/2\rho_0$, respectively, while the dotted line represents the parametrization of Cugnon *et al.* It is seen that at low energies and low densities, the parametrization of Cugnon *et al.* underestimates the microscopic results, while at higher energies and higher density it is the other way around. Note that the parametrization of Cugnon *et al.* is not density dependent and thus predicts the same for all densities.

Finally, we propose a parametrization for the total np cross section as a function of the incident energy $E_{\rm lab}$ and density ρ:

$$\sigma_{np}(E_{\rm lab},\rho) = [31.5 + 0.092\,{\rm abs}(20.2 - E_{\rm lab}^{0.53})^{2.9}] \times \frac{1.0 + 0.0034 E_{\rm lab}^{1.51}\rho^2}{1.0 + 21.55\rho^{1.34}}, \quad (15)$$

where $E_{\rm lab}$ and ρ are in the units of MeV and fm^{-3}, respectively.

We compare in Fig. 12 this parametrization (lines) with the microscopic results (points) based on Bonn A at four densities. It is seen that the parametrization reproduces well the microscopic results for energies and densities considered in this work.

V. SUMMARY AND OUTLOOK

In this paper, we presented a microscopic derivation of elastic in-medium NN scattering cross sections for energies up to 300 MeV and densities up to $2\rho_0$. This investigation is based upon the Bonn NN potential and the Dirac-Brueckner approach for nuclear matter.

The "bare" Bonn potential reproduces the free NN scattering cross sections (differential as well as total) accurately. When the potential is applied to nuclear mat-

ter using the Dirac-Brueckner approach, the saturation properties (saturation density and binding energy) are reproduced correctly. Thus, the Bonn model provides a good starting point for other investigations. The major conclusions of the present microscopic calculations are the following.

(1) There is strong density dependence for the in-medium cross sections. With the increase of density, the cross sections decrease. This indicates that a proper treatment of the density dependence of the in-medium NN cross sections is important.

(2) Our microscopic predictions differ from the commonly used parametrizations of the differential and the total cross sections developed by Cugnon *et al.* [72]. The parametrization of Cugnon *et al.* underestimates the anisotropy of the in-medium *np* differential cross sections. In the case of the total cross sections, the parametrization of Cugnon *et al.* either underestimates or overestimates the microscopic results, depending on energy and density.

At energies above 300 MeV, inelastic channels enter the picture. Microscopic models that also describe the inelasticity [9] have to be applied. These models will then also allow one to calculate the in-medium pion production. This is under investigation.

ACKNOWLEDGMENTS

One of the authors (G.Q.L.) gratefully acknowledges enlightening discussions with Prof. C. M. Ko. This work was supported in part by the U.S. National Science Foundation under Grant No. PHY-9211607, and by the Idaho State Board of Education.

[1] J. D. Walecka, Ann. Phys. (N.Y.) **83**, 491 (1974).
[2] B. D. Serot and J. D. Walecka, Adv. Nucl. Phys. **16**, 1 (1986).
[3] M. R. Anastasio, L. S. Celenza, W. S. Pong, and C. M. Shakin, Phys. Rep. **100**, 327 (1983).
[4] L. S. Celenza and C. M. Shakin, *Relativistic Nuclear Physics: Theories of Structure and Scattering*, Lecture Notes in Physics Vol. 2 (World Scientific, Singapore, 1986).
[5] R. Machleidt, Adv. Nucl. Phys. **19**, 189 (1989).
[6] R. Brockmann and R. Machleidt, Phys. Rev. C **42**, 1965 (1990).
[7] G. Q. Li, R. Machleidt, and R. Brockmann, Phys. Rev. C **45**, 2782 (1992).
[8] B. ter Haar and R. Malfliet, Phys. Rep. 149, 207 (1987).
[9] B. ter Haar and R. Malfliet, Phys. Rev. C **36**, 1611 (1987).
[10] R. Malfliet, Prog. Part. Nucl. Phys. **21**, 207 (1988).
[11] M. Brack, C. Guet, and H. B. Hakasson, Phys. Rep. **123**, 275 (1985).
[12] G. Q. Li, J. Phys. G **17**, 1 (1991).
[13] G. E. Brown and M. Rho, Phys. Rev. Lett. **66**, 2720 (1991).
[14] G. E. Brown M. Rho, and V. Koch, Nucl. Phys. **A535**, 701 (1991).
[15] T. Hatsuda and S. H. Lee, Phys. Rev. C **46**, R34 (1992).
[16] T. D. Cohen, R. J. Furnstahl, and D. K. Griegel, Phys. Rev. Lett. **67**, 961 (1991).
[17] M. Asakawa, C. M. Ko, P. Levai, and X. J. Qiu, Phys. Rev. C **46**, R1159 (1992).
[18] T. Izumoto, S. Krewald, and A. Faessler, Nucl. Phys. **A341**, 319 (1980).
[19] T. Izumoto, S. Krewald, and A. Faessler, Nucl. Phys. **A357**, 471 (1981).
[20] A. Faessler, Nucl. Phys. **A495**, 103c (1989).
[21] N. Ohtsuka, R. Linden, A. Faessler, and F. B. Malik, Nucl. Phys. **A465**, 550 (1987).
[22] A. Bohnet, N. Ohtsuka, J. Aichelin, R. Linden, and A. Faessler, Nucl. Phys. **A494**, 349 (1989).
[23] J. Jänicke, J. Aichelin, N. Ohtsuka, R. Linden, and A. Faessler, Nucl. Phys. **A536**, 201 (1992).
[24] G. Q. Li, Y. Lotfy, S. W. Huang, and A. Faessler, J. Phys. G **18**, 291 (1992).
[25] K. A. Brueckner, C. A. Levinson, and H. M. Mahmoud, Phys. Rev. **95**, 217 (1954).
[26] H. A. Bethe, Phys. Rev. **103**, 1352 (1956).
[27] J. Goldstone, Proc. R. Soc. London A **239**, 267 (1957).
[28] R. Jastrow, Phys. Rev. **98**, 1479 (1955).
[29] V. R. Pandharipande and R. B. Wiringa, Rev. Mod. Phys. **51**, 821 (1979).
[30] B. D. Day and R. B. Wiringa, Phys. Rev. C **32**, 1057 (1985).
[31] R. Stock, Phys. Rep. **135**, 259 (1986).
[32] H. Stöcker and W. Greiner, Phys. Rep. **137**, 278 (1986).
[33] G. F. Bertsch and S. Das Gupta, Phys. Rep. **160**, 189 (1988).
[34] W. Cassing, W. Metag, U. Mosel, and K. Niita, Phys. Rep. **188**, 363 (1990).
[35] J. Aichelin and H. Stöcker, Phys. Lett. B **176**, 14 (1986).
[36] J. Aichelin, Phys. Rep. **202**, 235 (1991).
[37] C. M. Ko, Q. Li, and R. C. Wang, Phys. Rev. Lett. **59**, 1084 (1987).
[38] B. Blättel, V. Koch, W. Cassing, and U. Mosel, Phys. Rev. C **38**, 1767 (1988).
[39] H. Sorge, H. Stöcker, and W. Greiner, Ann. Phys. (N.Y.) **192**, 266 (1989).
[40] T. Maruyama, S. W. Huang, N. Ohtsuka, G. Q. Li, A. Faessler, and J. Aichelin, Nucl. Phys. **A534**, 720 (1991).
[41] K. Niita, W. Cassing, and U. Mosel, Nucl. Phys. **A504**, 391 (1989).
[42] J. Q. Wu and C. M. Ko, Nucl. Phys. **A499**, 810 (1989).
[43] G. Q. Li, D. T. Khoa, T. Maruyama, S. W. Huang, N. Ohtsuka, A. Faessler, and J. Aichelin, Nucl. Phys. **A534**, 697 (1991).
[44] G. Q. Li, S. W. Huang, T. Maruyama, D. T. Khoa, Y. Lotfy, and A. Faessler, Nucl. Phys. **A537**, 645 (1992).
[45] R. Machleidt, K. Holinde, and Ch. Elster, Phys. Rep. **149**, 1 (1987).
[46] R. Vinh Mau, in *Mesons in Nuclei*, edited by M. Rho and D. H. Wilkinson (North-Holland, Amsterdam, 1979), Vol. I, p. 151.
[47] M. Lacombe, B. Loiseau, J. M. Richard, R. Vinh Mau, J. Cote, P. Pires, and R. de Tourreil, Phys. Rev. C **21**, 861 (1980).

[48] L. G. Arnold, B. C. Clark, and R. L. Mercer, Phys. Rev. C **19**, 917 (1979).
[49] S. Hama, B. C. Clark, E. D. Cooper, H. S. Sherif, and R. L. Mercer, Phys. Rev. C **41**, 2737 (1990).
[50] S. J. Wallace, Annu. Rev. Nucl. Part. Sci. **37**, 267 (1987).
[51] R. Brockmann and R. Machleidt, Phys. Lett. **149B**, 283 (1984).
[52] C. J. Horowitz and B. D. Serot, Phys. Lett. **137B**, 287 (1984).
[53] C. J. Horowitz and B. D. Serot, Nucl. Phys. **A464**, 613 (1987).
[54] H. Müther, R. Machleidt, and R. Brockmann, Phys. Rev. C **42**, 1981 (1990).
[55] R. Brockmann and H. Toki, Phys. Rev. Lett. **68**, 340 (1992).
[56] C. Nuppenau, A. D. MacKellar, and Y. J. Lee, Nucl. Phys. **A511**, 525 (1990).
[57] E. E. Salpeter and H. A. Bethe, Phys. Rev. C **84**, 1232 (1951).
[58] R. Blankendecler and R. Sugar, Phys. Rev. **142**, 1051 (1966).
[59] R. H. Thompson, Phys. Rev. D **1**, 110 (1970).
[60] R. Machleidt, in *Computational Nuclear Physics*, edited by S. E. Koonin, K. Langanke, and A. Maruhn (Springer, New York, 1993), Vol. II.
[61] J. D. Bjorken and S. D. Drell, *Relativistic Quantum Mechanics* (McGraw-Hill, New York, 1964).
[62] T. C. Montgomery, B. E. Bonner, F. P. Brady, W. B. Broste, and M. W. McNaughton, Phys. Rev. C **16**, 499 (1977).
[63] G. Fink *et al.* (unpublished).
[64] J. A. Edgington, V. J. Howard, I. M. Blair, B. E. Bonner, F. P. Brady, and M. W. McNaughton, Nucl. Phys. **A218**, 151 (1974).
[65] R. K. Keeler *et al.*, Nucl. Phys. **A377**, 529 (1982).
[66] A. Bol, P. Devescovi, P. Leleux, P. Lipnik, P. Macq, and J. P. Meulders, Phys. Rev. C **32**, 623 (1985).
[67] V. Grundies, J. Franz, E. Rössle, and H. Schmitt, Phys. Lett. **158B**, 15 (1985).
[68] P. W. Lisowski *et al.*, Phys. Rev. Lett. **49**, 255 (1982).
[69] G. Q. Li, R. Machleidt, and A. Faessler, in *Advances in Nuclear Dynamics: Proceedings of the Eighth Winter Workshop in Nuclear Dynamics*, edited by W. Bauer and B. Back (World Scientific, Singapore, 1992), p. 227.
[70] R. Machleidt and G. Q. Li, Invited talk presented at "Realistic Nuclear Structure," a conference to mark the 60th brithday of T. T. S. Kuo [Phys. Rep. (in press)].
[71] M. I. Haftel and F. Tabakin, Nucl. Phys. **A158**, 1 (1970).
[72] J. Cugnon, T. Mizutani, and J. Vandermeulen, Nucl. Phys. **A352**, 505 (1981).
[73] G. Q. Li and R. Machleidt, submitted to Phys. Rev. C.
[74] B. D. Day, Rev. Mod. Phys. **39**, 719 (1967); P. J. Siemens, Nucl. Phys. **A141**, 225 (1970); H. A. Bethe, Annu. Rev. Nucl. Sci. **21**, 93 (1971); see also Fig. 9.7 and Table 9.2 of Ref. [5].